INTERNATIONAL JOURNAL FOR NUMERICAL METHODS IN FLUIDS
Int. J. Numer. Meth. Fluids 2010; **62**:403–427
Published online 12 March 2009 in Wiley InterScience (www.interscience.wiley.com). DOI: 10.1002/fld.2024

A hybrid FVM–LBM method for single and multi-fluid compressible flow problems

Himanshu Joshi[1], Arpit Agarwal[2], Bhalchandra Puranik[1,*,†], Chang Shu[3] and Amit Agrawal[1]

[1]*Department of Mechanical Engineering, Indian Institute of Technology Bombay, Powai, Mumbai 400076, India*
[2]*Department of Mechanical Engineering, Massachusetts Institute of Technology, Cambridge, MA, U.S.A.*
[3]*Department of Mechanical Engineering, National University of Singapore, Singapore*

SUMMARY

The lattice Boltzmann method (LBM) has established itself as an alternative approach to solve the fluid flow equations. In this work we combine LBM with the conventional finite volume method (FVM), and propose a non-iterative hybrid method for the simulation of compressible flows. LBM is used to calculate the inter-cell face fluxes and FVM is used to calculate the node parameters. The hybrid method is benchmarked for several one-dimensional and two-dimensional test cases. The results obtained by the hybrid method show a steeper and more accurate shock profile as compared with the results obtained by the widely used Godunov scheme or by a representative flux vector splitting scheme. Additional features of the proposed scheme are that it can be implemented on a non-uniform grid, study of multi-fluid problems is possible, and it is easily extendable to multi-dimensions. These features have been demonstrated in this work. The proposed method is therefore robust and can possibly be applied to a variety of compressible flow situations. Copyright © 2009 John Wiley & Sons, Ltd.

Received 16 April 2008; Revised 30 January 2009; Accepted 1 February 2009

KEY WORDS: lattice Boltzmann method; finite volume method; Riemann solvers; Godunov method; compressible flow; multi-fluid flows

1. INTRODUCTION

The finite volume method (FVM) [1, 2] is widely used to solve fluid flow equations, including the compressible Euler equations. In FVM, volume integrals of the divergence terms in the governing partial differential equations are converted into surface integrals using the Gauss divergence theorem, which are then evaluated as surface fluxes. Several schemes have been proposed

*Correspondence to: Bhalchandra Puranik, Department of Mechanical Engineering, Indian Institute of Technology Bombay, Powai, Mumbai 400076, India.
†E-mail: puranik@iitb.ac.in

in the literature to obtain the surface fluxes (or inter-cell face parameters) from the given node parameters. The Godunov approach [2, 3] has been widely used to calculate the inter-cell face parameters, which are computed using the analytical solution of a localized Riemann problem. The Godunov scheme can accurately simulate the discontinuous waves but this method has a relatively higher computational cost. An analytical solution to the localized Riemann problem can be obtained using iterative methods such as the Newton–Raphson method but this approach has a still higher computational cost. In a practical computation, it may be required to solve the localized Riemann problem a large number of times, highlighting the need for computationally efficient solution schemes.

The computational efforts associated with an iterative method may not always be justified and therefore non-iterative solvers have been developed. Approximate non-iterative solvers have the potential to calculate the inter-cell face parameters for numerical purposes. Several approximate Riemann solvers have been proposed for approximating the inter-cell face parameters, and subsequently the physical fluxes at the inter-cell faces are calculated [4–7] from these approximate inter-cell face parameters. Although these approximate solvers are relatively easy to implement, they may not be sufficiently accurate. The solver proposed by Roe [4] is one of the most well-known approximate Riemann solvers and has been applied to a large variety of problems. Refinements to this approach were later introduced by Roe and Pike [5] and the new methodology was simpler and more useful in solving the Riemann problem. Further corrections to the basic Roe scheme have been proposed, but the solvers may fail to give the desired accuracy in complicated cases. Harten *et al*. [6] proposed the HLL Riemann solver which can directly approximate the inter-cell numerical fluxes without calculating the inter-cell parameters. The central idea of this method is to assume a two-wave configuration, which separates three constant states. This method is one of the more efficient and robust Riemann solvers, but the limitation of this method is the assumption of a two-wave configuration. As a consequence of this assumption, the resolution of physical features like the contact discontinuity may be inadequate. Some modifications to this solver have been proposed [7], but a number of limitations still remain.

Flux vector splitting (FVS) schemes can also be categorized as non-iterative Riemann solvers. The concept of FVS was first conceived by Steger and Warming [8]. Their scheme was based on splitting of eigenvalues of the jacobian matrix of the conservative form of the Euler equations. In order to overcome the numerical difficulties associated with sonic points, van Leer proposed a new FVS scheme [9]. Liou and Steffen [10] proposed the advection upstream splitting method (AUSM). Liou [11, 12] proposed sequels to AUSM: AUSM$^+$ and AUSM$^+$-up. The AUSM family of schemes was designed to avoid numerical mass diffusion at stagnation shown by the earlier FVS schemes. Zha and Bilgen [13] proposed another FVS scheme with the same objective as the AUSM scheme, and it is simpler in implementation than the AUSM scheme [13].

The lattice Boltzmann method (LBM) [14] is another numerical method that is often used to simulate flow problems. This method models fluid as a collection of particles, which successively undergo collision and propagation over a discrete lattice mesh. Several lattice Boltzmann models have been proposed for the incompressible Navier–Stokes equations [14, 15]. However in the author's experience [16], the usual collision–propagation method employed by the LBM cannot be used to solve the compressible Euler equations since this method is limited to flows with small Mach numbers. Several compressible lattice Boltzmann models have, however, been proposed in the literature [17–23]. Alexander *et al.* [17] proposed a lattice Boltzmann model with selectable

DOI: 10.1002/fld

sound speed to simulate compressible flows. In this model, the sound speed was set low by appropriately selecting the parameters of the distribution function. Yu and Zhao [18] suggested another model in which the sound speed is lowered by the introduction of an attractive force. Both of the above models are isothermal models and cannot simulate temperature profiles, and therefore cannot really be used as compressible flow solvers. Guangwu *et al.* [19] proposed a three-speed-three-energy-level lattice Boltzmann model for the compressible Euler equations. The specific heat ratio can be freely chosen in this 17 particle thermal model, but the method is computationally expensive as it assumes three different levels of velocity and temperature. The model of Kataoka and Tsutahara [20] is computationally less expensive than the three-speed-three-energy-level model, and has been adopted in the present work.

Another area which has received a great deal of attention is the numerical simulation of compressible multi-fluid flows. Such flows are relevant in nuclear power reactor safety analysis and find applications in different streams of engineering as well. In general, compressible multi-fluid flows are difficult to solve because additional parameters such as the ratio of specific heats (γ) and molecular mass (M) of the gases need to be appropriately modeled. The conventional 'gamma' and 'thermodynamic' models for multi-fluid flows fail to maintain the pressure equilibrium and result in oscillations and computational inaccuracies near the discontinuities and the material interfaces [24, 25]. One of the ways to tackle this issue is by introducing additional equations to describe the transport of ratio of specific heats (γ) and the molecular mass (M) of the gases along with the original Euler equations. Among other methods, a thermodynamically consistent and fully conservative method for multi-fluid flows is developed by Wang *et al.* [26]. The equations for mass fractions of each species and the ratio of specific heats of the mixture, proposed by Wang *et al.* [26], have been incorporated in this work.

The two numerical techniques, FVM and LBM, have some relative advantages over each other and provide a motivation to develop a hybrid FVM–LBM method for compressible flows by combining their relative strengths. It is desired that the new method should be computationally efficient and should accurately simulate all compressible flow features including shock, contact discontinuity and expansion wave. We show that the use of LBM for determining the inter-cell face fluxes, along with FVM at the nodes, gives a more accurate and efficient solver. This approach is first tested for a single-fluid flow and then extended to a multi-fluid problem by modifying the model of Kataoka and Tsutahara [20] suitably. The proposed hybrid scheme for single and multi-fluids is discussed in Sections 2 and 3, respectively. The numerical details pertinent to our implementation are summarized in Section 4. Details of the test cases are given in Section 5. A comparison between the results obtained from the hybrid method, the conventional Godunov method and the FVS scheme by Zha and Bilgen [13] is presented in Section 6. Final comments are presented in Section 7.

2. PROPOSED HYBRID FVM–LBM METHOD

The hybrid FVM–LBM method proposed here works on the fundamental idea that the LBM is used to determine the inter-cell face parameters and the conventional finite volume method is then used to calculate the node parameters.

The details of each of these steps in the hybrid method are now presented. The grid for the hybrid method is shown in Figure 1. All variables and equations are expressed in non-dimensional

DOI: 10.1002/fld

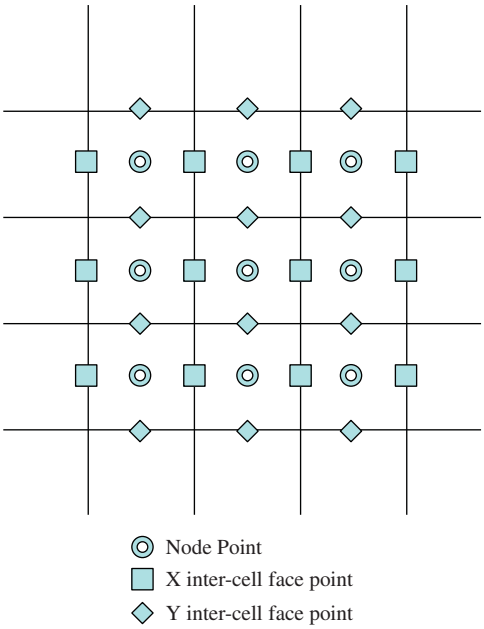

Figure 1. Grid structure for a two-dimensional problem indicating the nodes and the inter-cell face points.

form for the convenience of numerical calculation and analysis. Let L, $\hat{\rho}^{\mathrm{R}}$, and $\hat{T}^{\mathrm{R}}$ be the reference length, density and temperature, respectively. Then the non-dimensional variables are defined as follows [20]:

$$t=\frac{\hat{t}}{\dfrac{L}{\sqrt{R\hat{T}^{\mathrm{R}}}}},\quad x=\frac{\hat{x}}{L},\quad y=\frac{\hat{y}}{L}$$
$$\rho=\frac{\hat{\rho}}{\hat{\rho}^{\mathrm{R}}},\quad u_x=\frac{\hat{u}_x}{\sqrt{R\hat{T}^{\mathrm{R}}}},\quad u_y=\frac{\hat{u}_y}{\sqrt{R\hat{T}^{\mathrm{R}}}},\quad T=\frac{\hat{T}}{\hat{T}^{\mathrm{R}}},\quad p=\frac{\hat{p}}{\hat{\rho}^{\mathrm{R}}R\hat{T}^{\mathrm{R}}} \tag{1}$$

The symbols with '$\hat{}$' indicate the parameters in their dimensional form and without '$\hat{}$' indicate the same in their non-dimensional form. Furthermore, 't' denotes time, 'x' and 'y' spatial coordinates, 'T' temperature, 'p' pressure, 'ρ' density, 'u_x' velocity in x-direction, 'u_y' velocity in y-direction (all non-dimensional) and 'R' denotes specific gas constant.

FVM step: At the nodes, the two-dimensional time-dependent Euler equations in conservative form

$$U_t+F(U)_x+G(U)_y=0 \tag{2}$$

are solved using the standard finite volume approach. Here U is the vector of conserved variables, and $F(U)$ and $G(U)$ are the flux vectors along the x- and y-directions, respectively. These vectors

DOI: 10.1002/fld

are given as

$$U=\begin{bmatrix}\rho\\ \rho u_x\\ \rho u_y\\ E\end{bmatrix},\quad F(U)=\begin{bmatrix}\rho u_x\\ \rho u_x^2+p\\ \rho u_x u_y\\ u_x(E+p)\end{bmatrix},\quad G(U)=\begin{bmatrix}\rho u_y\\ \rho u_y u_x\\ \rho u_y^2+p\\ u_y(E+p)\end{bmatrix} \tag{3}$$

where 'E' is the total energy per unit volume given by

$$E=\rho(\tfrac{1}{2}(u_x^2+u_y^2)+e) \tag{4}$$

and 'e' denotes the specific internal energy. A conservative finite volume scheme for Equation (2) is of the form

$$U_{i,j}^{n+1}=U_{i,j}^{n}+\frac{\Delta t}{\Delta x}(F_{i-1/2,j}-F_{i+1/2,j})+\frac{\Delta t}{\Delta y}(G_{i,j-1/2}-G_{i,j+1/2}) \tag{5}$$

where $U_{i,j}^{n}$ denote the parameters at the node (i, j) and at time level n. The equation of state (in non-dimensional form) given by

$$p=\rho T \tag{6}$$

is required to be solved, along with Equation (2). Note that the specific gas constant 'R' disappears on non-dimensionalizing the equation of state. Calculation of numerical fluxes F and G required in Equation (5) needs calculation of flow parameters at the inter-cell faces.

LBM step: The flow parameters at the inter-cell faces are calculated using the lattice Boltzmann model by Kataoka and Tsutahara [20]. Details of this model are now presented. Here D is the total number of significant spatial dimensions and I is the total number of discrete molecular velocities.

(1) *One-dimensional model* ($D=1, I=5$): The macroscopic variables, i.e., density, velocity and temperature in a one-dimensional model are defined in terms of the particle velocity distribution function (f_k) as

$$\begin{aligned}\rho &= \sum_{k=1}^{I} f_k\\ \rho u &= \sum_{k=1}^{I} f_k c_{1k}\\ \rho(bT+u^2) &= \sum_{k=1}^{I} f_k(c_{1k}^2+\eta_k^2)\end{aligned} \tag{7}$$

where c_{1k} is the molecular velocity of the kth particle in the only significant direction, and the variable η_k has been introduced to control the ratio of specific heats. The constant b is expressed in terms of ratio of specific heats (γ) as

$$b=\frac{2}{(\gamma-1)} \tag{8}$$

DOI: 10.1002/fld

The molecular velocity is given by

$$c_{1k}=\begin{cases}0 & \text{for } k=1\\ v_1\cos(\pi k) & \text{for } k=2,3\\ v_2\cos(\pi k) & \text{for } k=4,5\end{cases} \tag{9}$$

and

$$\eta_k=\begin{cases}\eta_0 & \text{for } k=1\\ 0 & \text{for } k=2,3,4,5\end{cases} \tag{10}$$

where v_1, $v_2(\neq v_1)$ and η_0 are given non-zero constants.

The local equilibrium particle velocity distribution function (f_k^{eq}) is defined as

$$f_k^{\text{eq}}=\rho(A_k+B_k u c_{1k}) \quad \text{for } k=1,2,\ldots,5 \tag{11}$$

where

$$A_k=\begin{cases}\dfrac{(b-1)T}{\eta_0^2} & \text{for } k=1\\ \dfrac{1}{2(v_1^2-v_2^2)}\left[-v_2^2+\left((b-1)\dfrac{v_2^2}{\eta_0^2}+1\right)T+u^2\right] & \text{for } k=2,3\\ \dfrac{1}{2(v_2^2-v_1^2)}\left[-v_1^2+\left((b-1)\dfrac{v_1^2}{\eta_0^2}+1\right)T+u^2\right] & \text{for } k=4,5\end{cases} \tag{12a}$$

$$B_k=\begin{cases}\dfrac{-v_2^2+(b+2)T+u^2}{2v_1^2(v_1^2-v_2^2)} & \text{for } k=2,3\\ \dfrac{-v_1^2+(b+2)T+u^2}{2v_2^2(v_2^2-v_1^2)} & \text{for } k=4,5\end{cases} \tag{12b}$$

(2) *Two-dimensional model* ($D=2, I=9$): The macroscopic variables, i.e., density, velocity and temperature in a two-dimensional model are defined in terms of the particle velocity distribution function (f_k) as

$$\begin{aligned}\rho &= \sum_{k=1}^{I} f_k\\ \rho u_x &= \sum_{k=1}^{I} f_k c_{xk}\\ \rho u_y &= \sum_{k=1}^{I} f_k c_{yk}\\ \rho(bT+u_x^2+u_y^2) &= \sum_{k=1}^{I} f_k(c_{xk}^2+c_{yk}^2+\eta_k^2)\end{aligned} \tag{13}$$

DOI: 10.1002/fld

where c_{xk} and c_{yk} are the molecular velocities of the kth particle in the x- and y-directions, respectively. The molecular velocities are given by

$$(c_{xk}, c_{yk}) = \begin{cases} (0,0) & \text{for } k=1 \\ v_1\left(\cos\dfrac{\pi k}{2}, \sin\dfrac{\pi k}{2}\right) & \text{for } k=2,3,4,5 \\ v_2\left(\cos\dfrac{\pi(k+0.5)}{2}, \sin\dfrac{\pi(k+0.5)}{2}\right) & \text{for } k=6,7,8,9 \end{cases} \tag{14}$$

and

$$\eta_k = \begin{cases} \eta_0 & \text{for } k=1 \\ 0 & \text{for } k=2,3,\ldots,9 \end{cases} \tag{15}$$

where $v_1, v_2 (\neq v_1)$ and η_0 are given non-zero constants.

The local equilibrium particle velocity distribution function (f_k^{eq}) is defined as

$$f_k^{\text{eq}} = \rho(A_k + B_k(u_x c_{xk} + u_y c_{yk}) + D_k(u_x c_{xk} + u_y c_{yk})^2) \quad \text{for } k=1,2,\ldots,9 \tag{16}$$

where

$$A_k = \begin{cases} \dfrac{(b-2)T}{\eta_0^2} & \text{for } k=1 \\ \dfrac{1}{4(v_1^2 - v_2^2)}\left[-v_2^2 + \left((b-2)\dfrac{v_2^2}{\eta_0^2} + 2\right)T + \dfrac{v_2^2}{v_1^2}(u_x^2 + u_y^2)\right] & \text{for } k=2,3,4,5 \\ \dfrac{1}{4(v_2^2 - v_1^2)}\left[-v_1^2 + \left((b-2)\dfrac{v_1^2}{\eta_0^2} + 2\right)T + \dfrac{v_1^2}{v_2^2}(u_x^2 + u_y^2)\right] & \text{for } k=6,7,8,9 \end{cases} \tag{17a}$$

$$B_k = \begin{cases} \dfrac{-v_2^2 + (b+2)T + u_x^2 + u_y^2}{2v_1^2(v_1^2 - v_2^2)} & \text{for } k=2,3,4,5 \\ \dfrac{-v_1^2 + (b+2)T + u_x^2 + u_y^2}{2v_2^2(v_2^2 - v_1^2)} & \text{for } k=6,7,8,9 \end{cases} \tag{17b}$$

$$D_k = \begin{cases} \dfrac{1}{2v_1^4} & \text{for } k=2,3,4,5 \\ \dfrac{1}{2v_2^4} & \text{for } k=6,7,8,9 \end{cases} \tag{17c}$$

The particle kinetic equation used to solve for the particle velocity distribution function at the new time level is given as

$$\frac{\partial f_k}{\partial t} + c_{xk}\frac{\partial f_k}{\partial x} + c_{yk}\frac{\partial f_k}{\partial y} = \frac{f_k^{\text{eq}}(\rho, u_x, u_y, T) - f_k}{\varepsilon} \tag{18}$$

DOI: 10.1002/fld

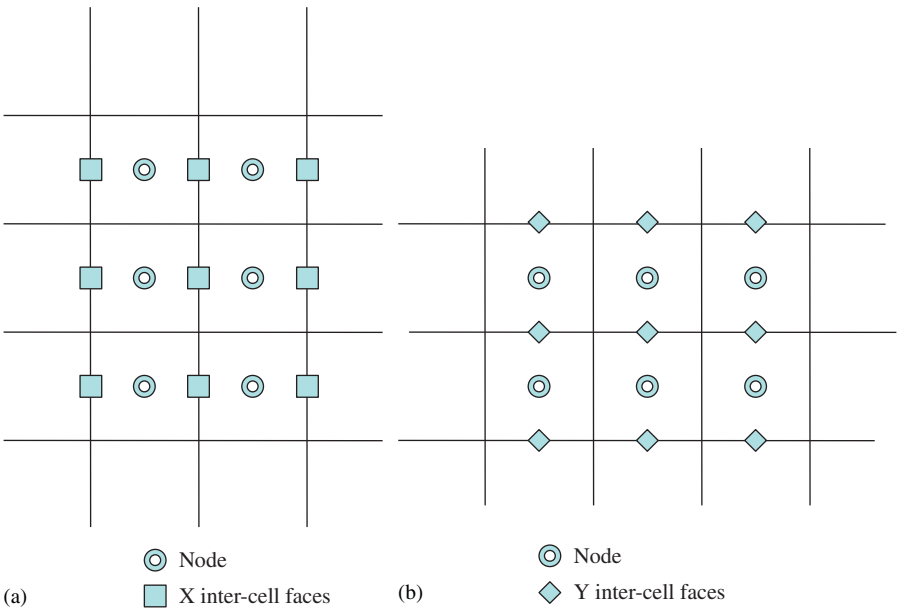

Figure 2. (a) Grid structure for obtaining the X inter-cell face parameter values by LBM and (b) grid structure for obtaining the Y inter-cell face parameter values by LBM.

where ε is the Knudsen number. The velocity distribution function at the old time step is obtained from the equilibrium velocity distribution function (f_k^{eq}), i.e.,

$$f_k^o = f_k^{\mathrm{eq}}(\rho^o, u_x^o, u_y^o, T^o) \tag{19}$$

where the superscript 'o' denotes the function at the previous time step.

This completes the description of the lattice Boltzmann model. Note that the particle kinetic equation (Equation (18)) has been written for a two-dimensional model. For one-dimensional case, only one of the convective terms corresponding to the only significant direction, is considered.

Implementation details of the LBM are now presented. The grid used to solve the particle kinetic equation is shown in Figure 2. The grid in Figure 2(a) is used to calculate the X inter-cell face parameters, while the grid in Figure 2(b) is used to calculate the Y inter-cell face parameters. LBM is applied separately on both these grids. Details are given for X inter-cell face parameters calculation; Y inter-cell face parameters calculation follows the same steps. At the beginning of every time step, velocity distribution function at the old time step is obtained by the use of Equations (9)–(12) (for one-dimensional model) or Equations (14)–(17) (for two-dimensional model) and Equation (19) at every point (both node and inter-cell face points) of the grid shown in Figure 2(a). A discretized form of the particle kinetic equation (Equation (18)) is used at the inter-cell face points to obtain the particle velocity distribution function at the new time step. Macroscopic variables at the inter-cell faces are then obtained from this new particle velocity

DOI: 10.1002/fld

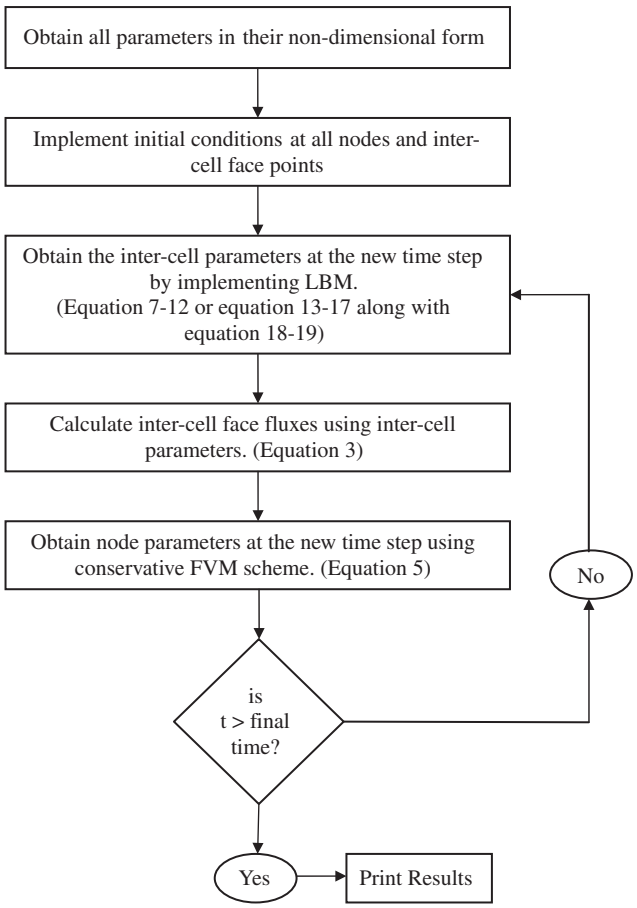

Figure 3. Flowchart showing the basic steps in the proposed hybrid FVM–LBM method.

distribution function by the use of Equation (7) (for one-dimensional model) or Equation (13) (for two-dimensional model).

The essential procedure in this hybrid method is now presented. This procedure is also summarized in Figure 3.

1. Initial conditions, i.e., the velocity, pressure, density and temperature expressed in their non-dimensional forms are assigned to the nodes and to the inter-cell faces (both X and Y inter-cell faces).
2. The macroscopic parameter values are obtained for the X and Y inter-cell faces, at the next time step by implementing the LBM model.
3. The inter-cell fluxes F and G are calculated at each inter-cell face from the flow parameter values at that face, using Equation (3).
4. Equation (5) is used to update the node parameters from time level n to time level $(n+1)$.

Steps 2–4 are repeated until the output time has reached.

DOI: 10.1002/fld

3. EXTENSION OF THE HYBRID FVM–LBM METHOD FOR MULTI-FLUID FLOWS

We use the hybrid FVM–LBM method, which was introduced in the previous section, for the simulation of multi-fluid flows. A comparison with the FVM–Godunov scheme for multi-fluid flows is presented in Section 6.4. As discussed earlier, an extended system with additional equations besides the original Euler equations has been proposed by Wang *et al.* [26]. This system involves two additional formulations for the calculation of the ratio of specific heat of the mixture and the molecular mass of the mixture. These formulations are given by

$$\frac{\partial}{\partial t}\left(\frac{1}{M}\rho\right)+\nabla\cdot\left(\frac{1}{M}\rho u\right)=0 \tag{20}$$

and

$$\frac{\partial}{\partial t}(\chi\rho)+\nabla\cdot(\chi\rho u)=0 \tag{21}$$

where 'M' is the molecular mass of the mixture and 'χ' is the ratio of specific heats at constant pressure to the specific gas constant and can be expressed in terms of the ratio of specific heats as

$$\chi=\frac{\gamma}{(\gamma-1)} \tag{22}$$

Therefore, the complete multi-fluid model involves modifying the vectors $U, F(U)$ and $G(U)$ in Equation (3) to

$$U=\begin{bmatrix}\rho\\ \rho u_x\\ \rho u_y\\ E\\ \rho/M\\ \chi\rho\end{bmatrix},\quad F(U)=\begin{bmatrix}\rho u_x\\ \rho u_x^2+p\\ \rho u_x u_y\\ u_x(E+p)\\ \rho u_x/M\\ \chi\rho u_x\end{bmatrix},\quad G(U)=\begin{bmatrix}\rho u_y\\ \rho u_y u_x\\ \rho u_y^2+p\\ u_y(E+p)\\ \rho u_y/M\\ \chi\rho u_y\end{bmatrix} \tag{23}$$

For a single gas, the required inter-cell fluxes were obtained using LBM; we maintain the same approach for multi-fluid flows as well. The model of Kataoka and Tsutahara [20] is applicable only for a single-gas flow. We modify the model suitably for multi-fluid problems.

We define a slightly modified set of non-dimensional variables in terms of the reference length (L), reference density ($\hat{\rho}^{\mathrm{R}}$), reference specific gas constant ($\hat{R}^{\mathrm{R}}$) and reference temperature ($\hat{T}^{\mathrm{R}}$). The new set of non-dimensional variables for multi-fluid flows is

$$\begin{aligned}&t=\frac{\hat{t}}{\dfrac{L}{\sqrt{\hat{R}^{\mathrm{R}}\hat{T}^{\mathrm{R}}}}},\quad x=\frac{\hat{x}}{L},\quad y=\frac{\hat{y}}{L}\\ &\rho=\frac{\hat{\rho}}{\hat{\rho}^{\mathrm{R}}},\quad u_x=\frac{\hat{u}_x}{\sqrt{\hat{R}^{\mathrm{R}}\hat{T}^{\mathrm{R}}}},\quad u_y=\frac{\hat{u}_y}{\sqrt{\hat{R}^{\mathrm{R}}\hat{T}^{\mathrm{R}}}},\quad T=\frac{\hat{R}\hat{T}}{\hat{R}^{\mathrm{R}}\hat{T}^{\mathrm{R}}},\quad p=\frac{\hat{p}}{\hat{\rho}^{\mathrm{R}}\hat{R}^{\mathrm{R}}\hat{T}^{\mathrm{R}}}\end{aligned} \tag{24}$$

DOI: 10.1002/fld

It can be observed that an additional parameter (reference specific gas constant) is used for obtaining the multi-fluid flow parameters in their non-dimensional form. In essence, the primary modification incorporated in the new model, which seems to make it suitable for multi-fluid flows, is that the variable T has been replaced by the variable RT in Equations (7)–(19). This modified model can now be used to calculate the inter-cell face parameters from the node parameters as discussed earlier.

In the multi-fluid problem solved here, the extended Euler equations (Equations (2) and (23)), are solved at the nodes along with Equations (7)–(12) (for one-dimensional model) or Equations (13)–(17) (for two-dimensional model) in their modified form, at the interfaces. While the γ-equation (Equation (21)) allows for the variation in the ratio of specific heats, the variation in the total energy is taken into account through the energy equation. To calculate the temperature of the gases, one needs to calculate the molecular mass using Equation (20), from where the specific gas constant is obtained. Knowing the variation of both RT and R, the variation of T can be calculated.

4. COMPUTATIONAL DETAILS

The computational details pertaining to the hybrid method are presented in this section. The parameters in LBM equations are chosen to be $v_1=1$, $v_2=3$, $\eta_0=2$. The discretized form of the particle kinetic equation (Equation (18)) is obtained by assuming the RHS to be identically equal to zero and assuming the derivative approximations to be first-order forward in time and first-order upwind in space. The final form of the discretized kinetic equation used is

$$(f_k)_{i,j}^{n+1}=(f_k)_{i,j}^{n}-\Delta t\left[\frac{(c_{xk}+|c_{xk}|)}{2}\left(\frac{(f_k)_{i,j}^{n}-(f_k)_{i-1,j}^{n}}{\Delta X}\right)-\frac{(c_{xk}-|c_{xk}|)}{2}\left(\frac{(f_k)_{i,j}^{n}-(f_k)_{i+1,j}^{n}}{\Delta X}\right)\right]$$
$$-\Delta t\left[\frac{(c_{yk}+|c_{yk}|)}{2}\left(\frac{(f_k)_{i,j}^{n}-(f_k)_{i,j-1}^{n}}{\Delta Y}\right)-\frac{(c_{yk}-|c_{yk}|)}{2}\left(\frac{(f_k)_{i,j}^{n}-(f_k)_{i,j+1}^{n}}{\Delta Y}\right)\right] \quad (25)$$

For the grid shown in Figure 2(a), $\Delta X=\Delta x/2$ and $\Delta Y=\Delta y$. For the grid shown in Figure 2(b), $\Delta X=\Delta x$ and $\Delta Y=\Delta y/2$. A transmissive boundary condition [2] has been implemented on all domain boundaries for all test problems.

Choice of time step: Kataoka and Tsutahara [20] proved that the dimensionless mesh width $(\Delta t, \Delta x, \Delta y)$ has to be much smaller than ε (Knudsen number) to assure the consistency of the finite difference scheme with the original kinetic equation. This means that the time step is restricted to a much smaller value in LBM. In FVM, the time step is restricted using the Courant–Friedrichs–Lewy (CFL) criterion so that waves generated at any inter-cell face location do not reach the next face location. In general, FVM can have much larger time steps than the LBM. In the hybrid method we have utilized this advantage of the FVM. The time step is decided based on CFL criterion given by [2]

$$\Delta t=C_{\mathrm{cfl}}\times\min\left(\frac{\Delta x_{i,j}}{S_{i,j}^{n,x}},\frac{\Delta y_{i,j}}{S_{i,j}^{n,y}}\right) \quad (26)$$

DOI: 10.1002/fld

where C_{cfl} is the CFL coefficient and $S_{i,j}^{n,\alpha}$ is the wave speed in the α-direction. Here, C_{cfl} is chosen as $0<C_{\text{cfl}}<0.5$ since the grid spacing in Figure 2(a) is $(\Delta x/2)$ and in Figure 2(b) is $(\Delta y/2)$. Since the wave speeds are not calculated explicitly in LBM, the most popular choice for wave speed [2], which extends to multi-dimensions can be used

$$S_{i,j}^{n,\alpha}=|V_{i,j}^{n}|+a_{i,j}^{n} \tag{27}$$

where $V_{i,j}^{n}$ is the macroscopic velocity component in α-direction and $a_{i,j}^{n}$ is the speed of sound at time level n, in cell $[i, j]$.

A grid independence test has been carried out to determine the appropriate grid spacing. Test case 3 of Section 5.1 has been solved with three different grid spacings: 0.01, 0.02 and 0.04 (Figures 4–6). The grid spacing of 0.04 results in a significant numerical diffusion and a comparatively lesser steep shock and contact discontinuity waves (Figure 4). On the other hand, the grid spacing of 0.01 produces accurate results (Figure 5), but it requires a large computational cost. Therefore, the grid spacing (Δx) has been chosen to be 0.02 (Figure 6) as reasonably accurate results can be generated with this Δx at an acceptable computational cost.

5. TEST CASES

A brief description of the test cases is presented in this section.

5.1. One-dimensional test cases

The hybrid method is benchmarked for several one-dimensional Riemann problems that have exact solution. A Riemann problem consists of a conservation law together with a piecewise constant initial data having a single discontinuity. The Riemann problem for one-dimensional time-dependent Euler equations is represented as the conservation law

$$U_t+F(U)_x=0 \tag{28}$$

with the initial conditions given as

$$U(x,0)=\begin{cases} U_L & \text{if } x<0 \\ U_R & \text{if } x>0 \end{cases} \tag{29}$$

where U is the vector of conserved variables and $F(U)$ is the flux vector.

Table I shows the initial conditions on either side of the initial discontinuity for the four test cases considered. The four test cases produce (i) two shock waves, (ii) two expansion waves, (iii) a left shock wave and a right expansion wave, and (iv) a left expansion wave and a right shock wave, respectively. The last column in Table I shows the non-dimensional output time at which results are plotted for the test case. The grid spacing used for all four test cases, based on grid independence study presented in Section 4, is 0.02.

5.2. Two-dimensional test cases

Two test cases are used for two-dimensional formulation.

DOI: 10.1002/fld

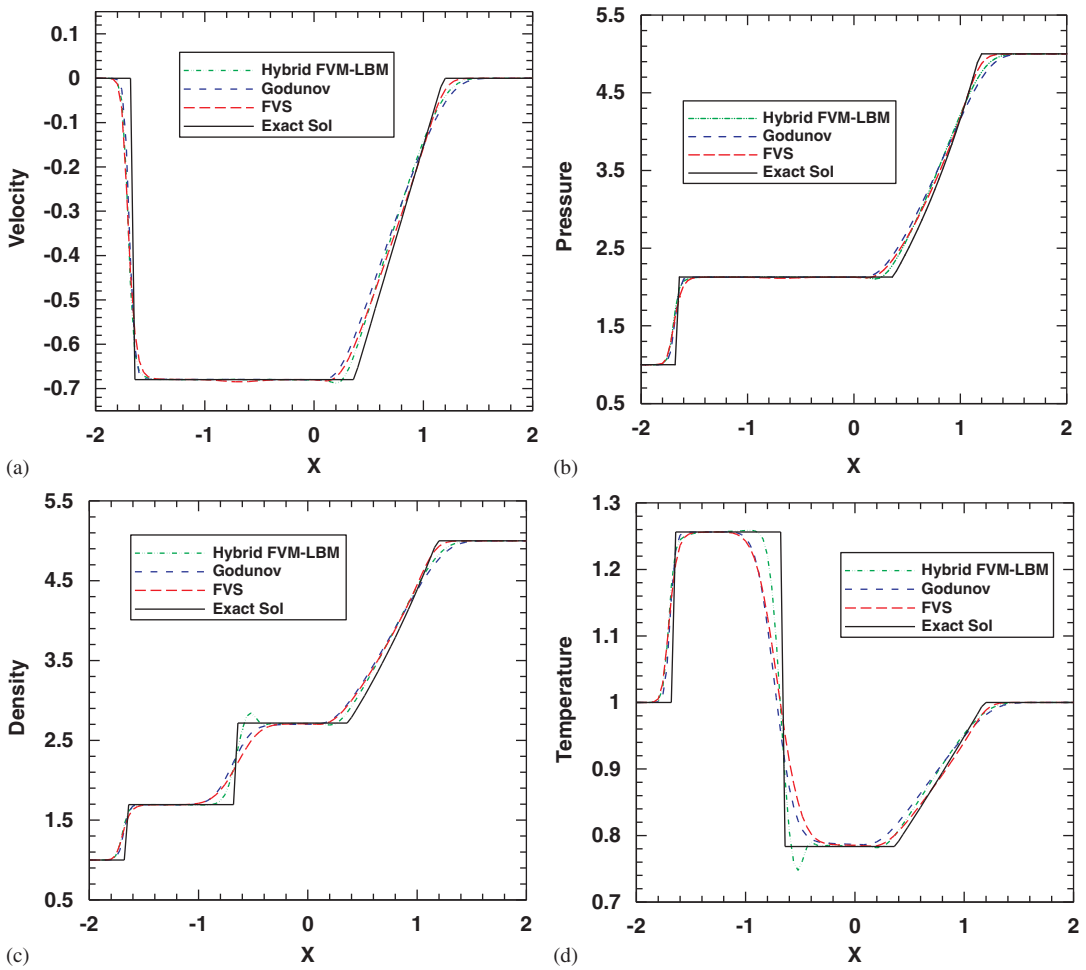

Figure 4. Results for Test case 3 (Section 5.1) after time $t=1$ ($\Delta x=0.04, \gamma=1.4$) for non-dimensional: (a) velocity; (b) pressure; (c) density; and (d) temperature.

5.2.1. Two-dimensional Riemann problem. This is also called the four-quadrant problem. In the Riemann problems for two-dimensional gas dynamics, the initial data are constant in each quadrant and so restricted that only one elementary wave: a one-dimensional shock, a one-dimensional rarefaction wave or a two-dimensional slip line (contact discontinuity) appears at each interface. Lax and Liu [27] have shown that there are 19 genuinely different configurations of this problem for a polytropic gas based on different combinations of elementary waves. Results for configurations 8 and 12 from Lax and Liu [27] are shown in Section 6.3.1. Other configurations (not presented) also show satisfactory results. Initial conditions for above two configurations are given in Table II.

For the configuration-8, four elementary waves are as follows:

1. An expansion wave moving towards left appears at the interface between quadrants 1 and 2.
2. A negative slip line appears at the interface between quadrants 2 and 3.

DOI: 10.1002/fld

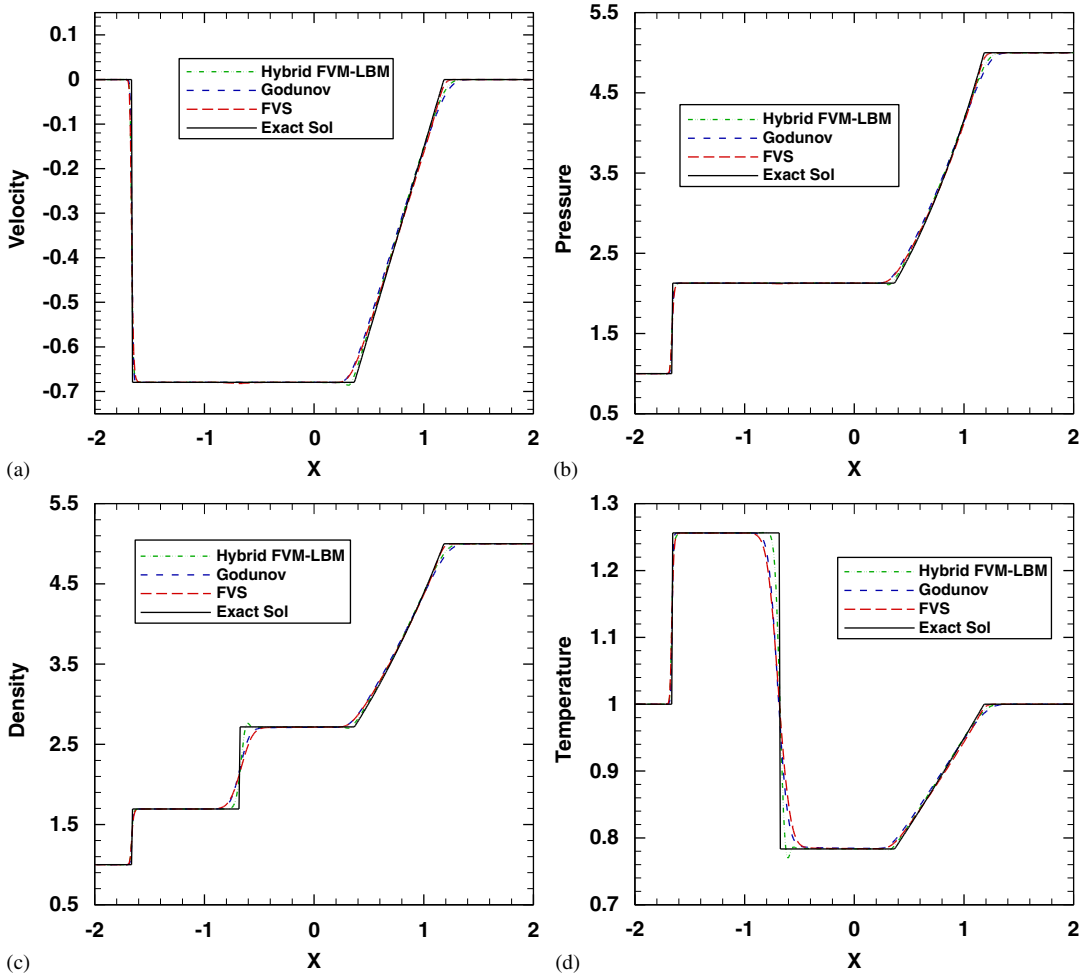

Figure 5. Results for Test case 3 (Section 5.1) after time $t=1$ ($\Delta x=0.01, \gamma=1.4$) for non-dimensional: (a) velocity; (b) pressure; (c) density; and (d) temperature.

3. A negative slip line appears at the interface between quadrants 3 and 4.
4. An expansion wave moving downwards appears at the interface between quadrants 1 and 4.

For the configuration-12, four elementary waves are as follows:

1. A shock wave moving towards right appears at the interface between quadrants 1 and 2.
2. A positive slip line appears at the interface between quadrants 2 and 3.
3. A positive slip line appears at the interface between quadrants 3 and 4.
4. A shock wave moving upwards appears at the interface between quadrants 1 and 4.

The non-dimensional output time for both these configurations is 0.25. A grid spacing of $\Delta x=\Delta y=0.0025$ is used for these problems.

DOI: 10.1002/fld

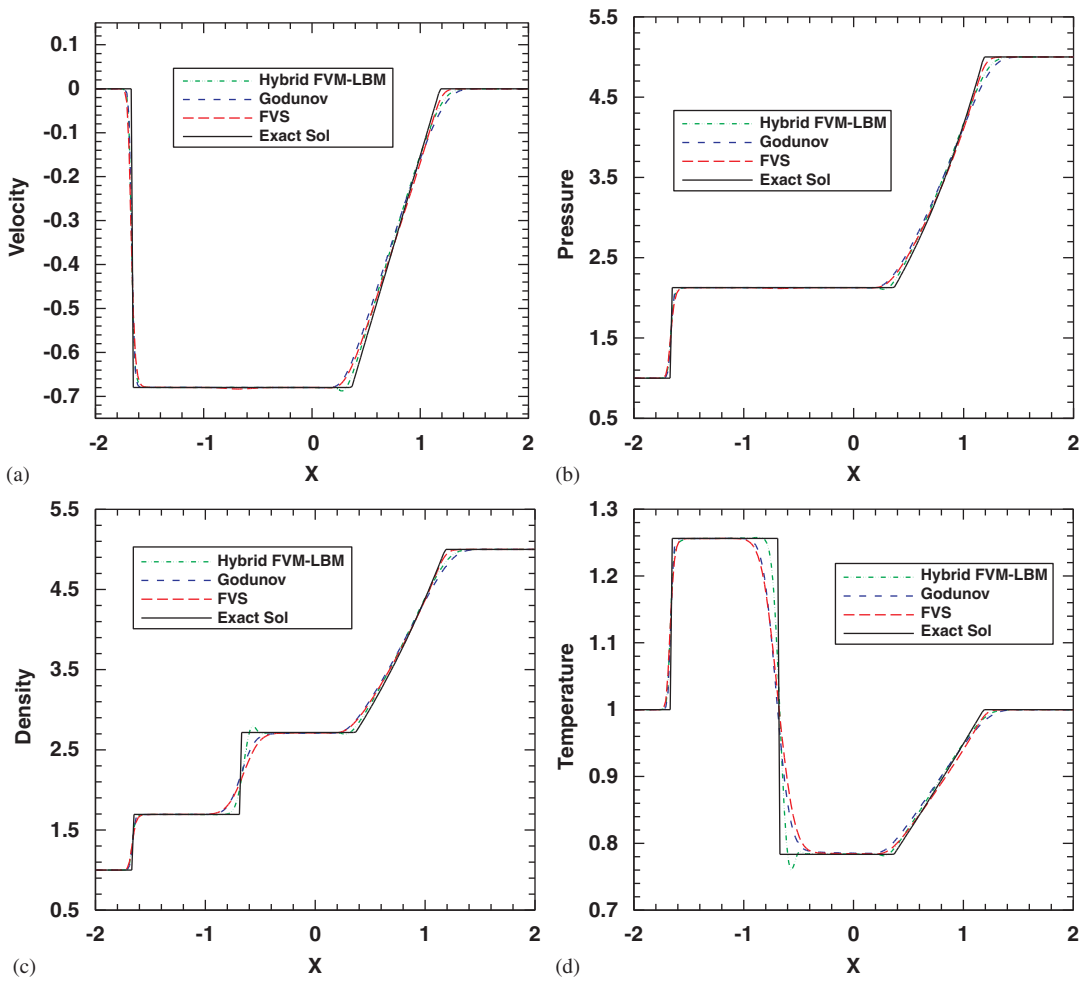

Figure 6. Results for Test case 3 (Section 5.1) after time $t=1$ ($\Delta x=0.02, \gamma=1.4$) for non-dimensional: (a) velocity; (b) pressure; (c) density; and (d) temperature.

Table I. Input data for one-dimensional test cases.

Test	T_L	u_L	ρ_L	T_R	u_R	ρ_R	Output time
1	1.000	1.000	1.000	1.000	−1.000	1.000	1.000
2	1.800	−1.000	1.000	1.800	1.000	1.000	0.200
3	1.000	0.000	1.000	1.000	0.000	5.000	1.000
4	1.000	0.000	1.000	0.800	0.000	0.125	0.800

DOI: 10.1002/fld

Table II. Initial conditions for four-quadrant problem.

	Configuration-8				Configuration-12			
Quadrant	ρ	u_x	u_y	T	ρ	u_x	u_y	T
1st	0.5197	0.1	0.1	0.76968	0.5313	0	0	0.75287
2nd	1	−0.6259	0.1	1	1	0.7276	0	1
3rd	0.8	0.1	0.1	1.25	0.8	0	0	1.25
4th	1	0.1	−0.6259	1	1	0	0.7276	1

5.2.2. Shock- square cylinder interaction. In this problem a shock generated in the one-dimensional Test case-4 is made to interact with a solid square cylinder. Reflection of the shock from the front face and diffraction over the rear corners are studied as time progresses. The initial position of the shock in the domain is taken at $x=0.3$. A solid square cylinder (of dimension $L=B=0.1$) is placed at the centre of the computational domain. Grid spacing of $\Delta x=\Delta y=0.01$ is used for this problem. Reflective boundary condition [2] by the use of fictitious cells is implemented on the cylinder walls, whereas transmissive boundary condition [2] is used on the computational domain boundaries.

5.3. Multi-fluid test problem

The hybrid scheme is benchmarked for a multi-fluid shock tube, which contains different gases in the two sections of the shock tube, separated by a diaphragm. The initial parameters on the left and right side of the diaphragm are:

$$(\rho_L, u_L, T_L, \gamma_L, R_L = 1, 0, 1, \tfrac{7}{5}, 1), \quad x<0$$

$$(\rho_R, u_R, T_R, \gamma_R, R_R = 5, 0, 1, \tfrac{9}{7}, 0.8), \quad x>0$$

6. RESULTS AND DISCUSSION

The results obtained with the hybrid method have been compared with the results from the FVM–Godunov scheme, the FVS scheme of Zha and Bilgen and the exact analytical solution for all one-dimensional test cases with single-fluid compressible flows. The results for single-fluid flows are first discussed in Sections 6.1–6.3. Section 6.4 includes the results for the two-gas shock tube.

6.1. Results for one-dimensional single-fluid compressible flows

6.1.1. Test case 1. This Riemann problem generates a flow with steep variations. The wave structure consists of two shock waves moving on the either side of the initial discontinuity. The contact discontinuity wave is absent in this problem. The hybrid FVM–LBM method simulates accurate shock profiles for this Riemann problem, which is evident by comparing against the analytical results (Figure 7). Furthermore, comparison between the results obtained using the FVM–Godunov method, the FVS scheme of Zha and Bilgen and the hybrid FVM–LBM method with the exact solution shows that the hybrid method simulates the shock profiles more accurately.

DOI: 10.1002/fld

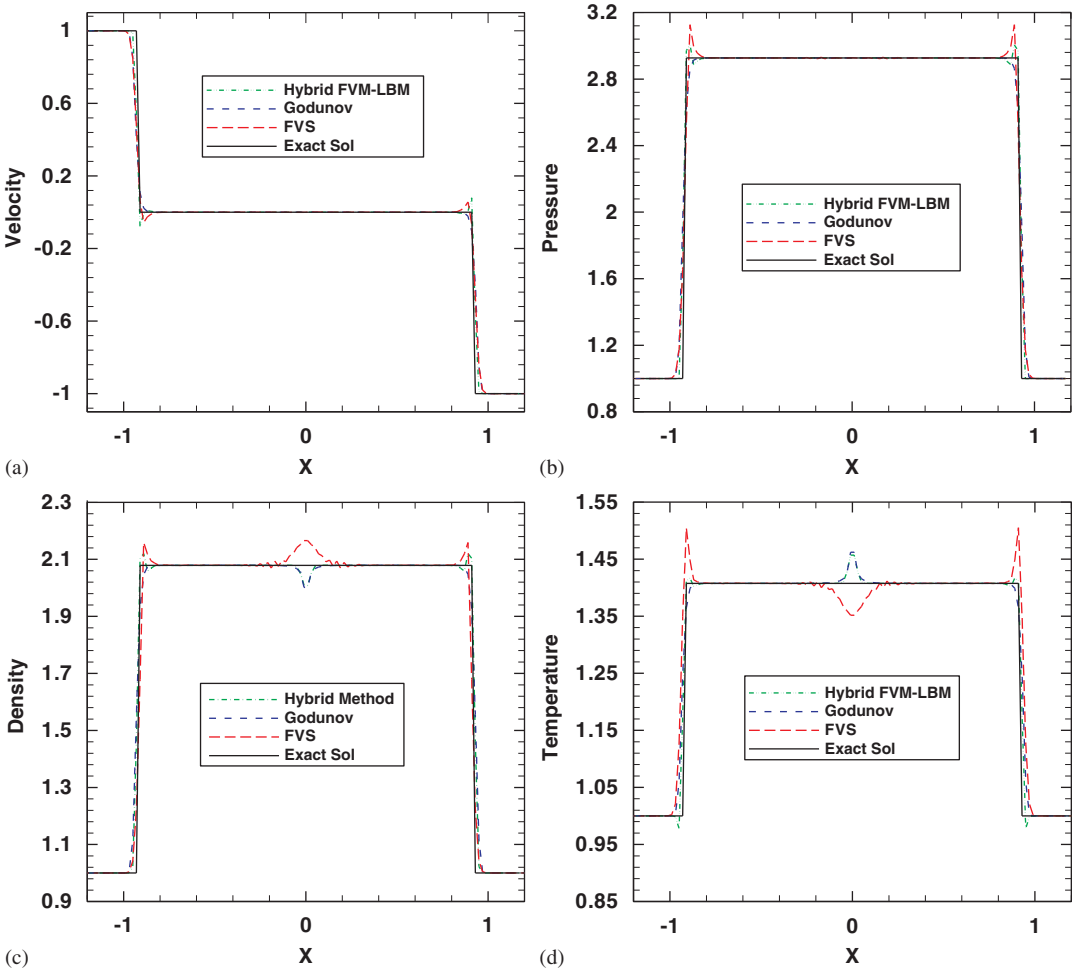

Figure 7. Results for Test case 1 (Section 5.1) after time $t=1$ ($\Delta x=0.02, \gamma=1.4$) for non-dimensional: (a) velocity; (b) pressure; (c) density; and (d) temperature.

6.1.2. Test case 2. The solution to this test consists of two expansion waves moving on either side of the initial discontinuity. The contact discontinuity wave is absent in this problem as well. The results obtained using the FVM–Godunov method, the FVS scheme of Zha and Bilgen, the hybrid FVM–LBM method and the exact solution are shown in Figure 8. The results indicate that the hybrid method simulates the expansion wave profiles more accurately.

6.1.3. Test case 3. This is the shock tube test case. When the diaphragm is broken ($t=0$), a shock wave propagates in the left section and an expansion wave propagates in the right. The results are shown in Figure 6. The hybrid method simulates the shock wave, the contact discontinuity and the expansion wave more accurately as compared with the FVM–Godunov method and the FVS scheme of Zha and Bilgen.

DOI: 10.1002/fld

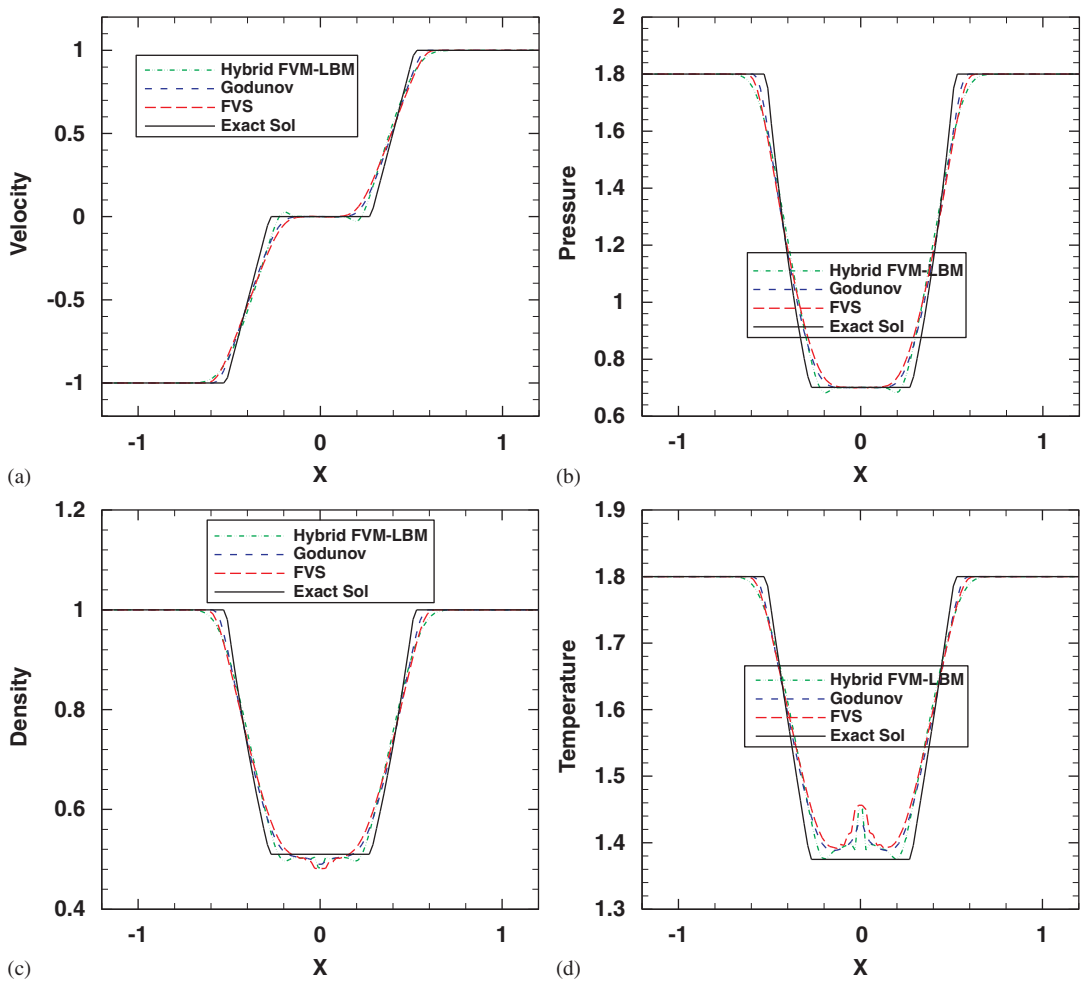

Figure 8. Results for Test case 2 (Section 5.1) after time $t=0.2$ ($\Delta x=0.02, \gamma=1.4$) for non-dimensional: (a) velocity; (b) pressure; (c) density; and (d) temperature.

6.1.4. Test case 4. This test case is also a shock tube test case. When the diaphragm is broken ($t=0$), a shock wave propagates in the right section and an expansion wave propagates in the left. The results obtained are shown in Figure 9. Once again, it is clear from the results that hybrid method simulates the shock wave, the contact discontinuity and the expansion wave more accurately as compared with the FVM–Godunov method and the FVS scheme of Zha and Bilgen.

6.2. Shock tube problem on a non-uniform grid

The purpose of this section is to show that the hybrid method can also be used with non-uniform grids. Although our formulation employs LBM, it does not require a uniform grid structure. This is evident from the results shown in Figure 10, where Test case 4 of Section 5.1 has been

DOI: 10.1002/fld

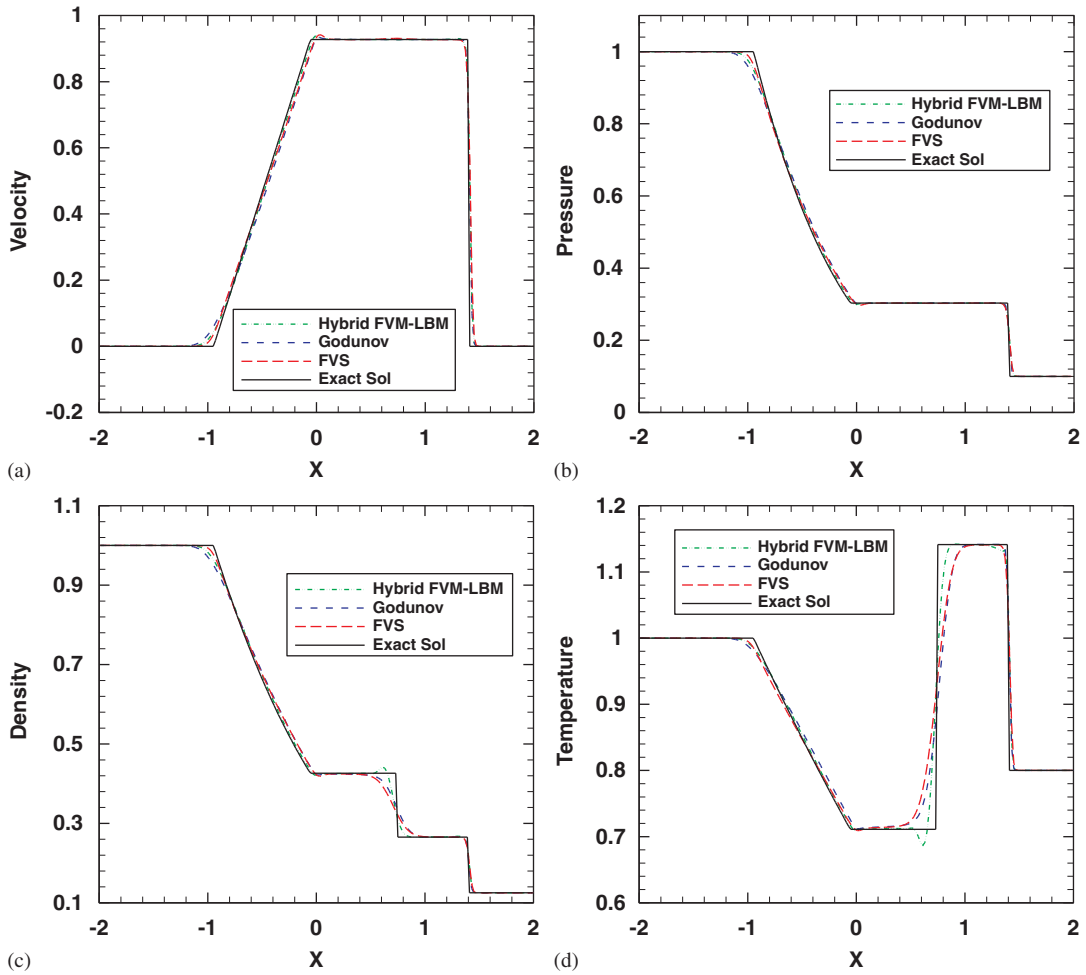

Figure 9. Results for Test case 4 (Section 5.1) after time $t=0.8$ ($\Delta x=0.02, \gamma=1.4$) for non-dimensional: (a) velocity; (b) pressure; (c) density; and (d) temperature.

re-solved on a non-uniform grid. The non-uniform grid is generated in the following manner: the domain is discretized into 250 computational cells; 125 cells on each side of initial discontinuity which is taken at $x=0$. The grid is symmetric on both sides of $x=0$. The first cell on either side has $\Delta x=0.0076$. The cell length then increases by 0.0002 with each cell, away from the point of symmetry. The extreme left and extreme right cells have $\Delta x=0.0324$. On comparing Figures 9 and 10, it is clear that similar accuracy in results is obtained with non-uniform grids as well. These results are significant because generally LBM has been applied with uniform grids.

6.3. Results for two-dimensional single-fluid compressible flows

6.3.1. Two-dimensional Riemann problem. The density contours after time $t=0.25$ obtained using the hybrid method for configuration-8 are shown in Figure 11(a). Two expansion waves can be

DOI: 10.1002/fld

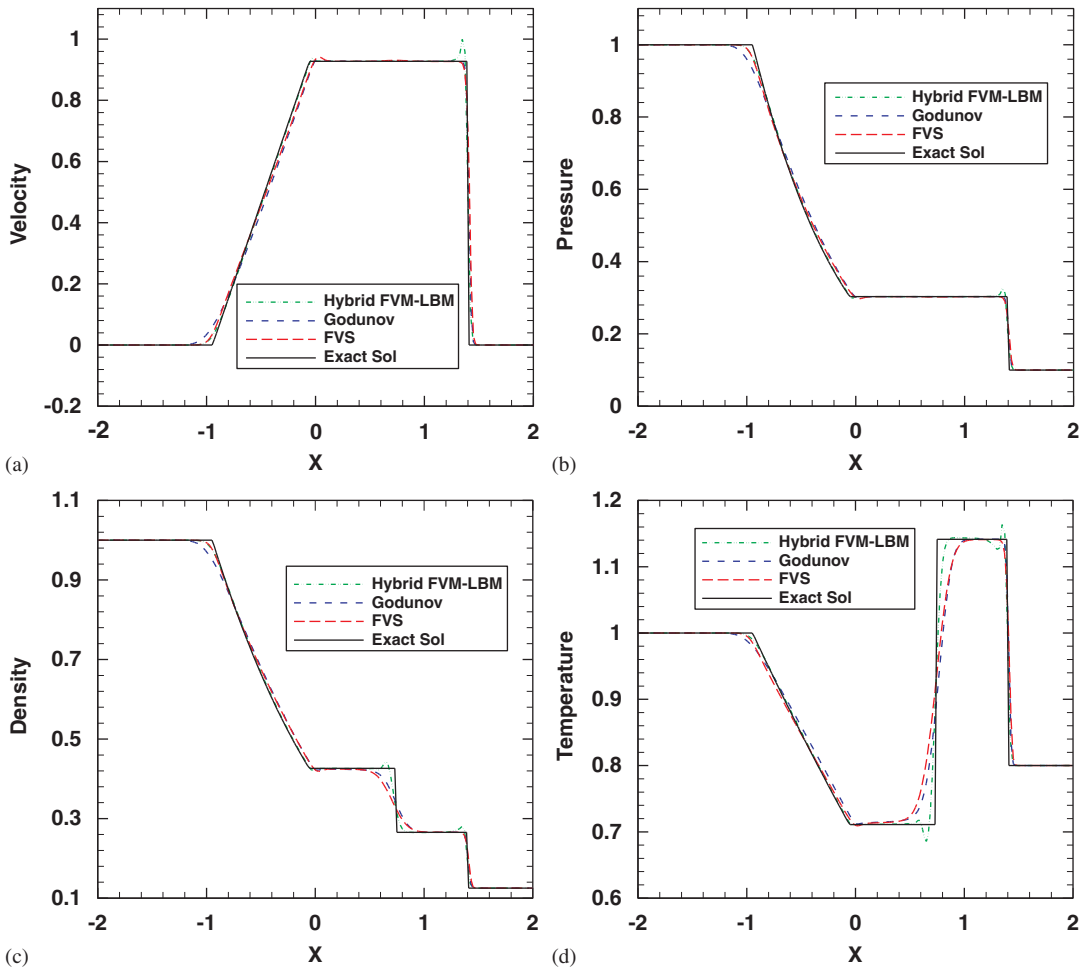

Figure 10. Results for Test case 4 (Section 5.1) on non-uniform grid ($t=0.8, \gamma=1.4$) for non-dimensional: (a) velocity; (b) pressure; (c) density; and (d) temperature.

seen in the second and fourth quadrants and two slip lines are also visible in the domain. The density contours for this configuration obtained by Lax and Liu [27] are shown in Figure 11(b) for comparison. The density contours after time $t=0.25$ obtained using the hybrid method for configuration-12 are shown in Figure 11(c). Two shock waves can be seen in the first quadrant. One slip line is seen along the interface between the second and the third quadrant and the other slip line along the interface between the third and the fourth quadrant. The corresponding results obtained by Lax and Liu [27] are shown in Figure 11(d) for comparison. From the comparison presented in Figure 11, it is evident that the hybrid method works well for a two-dimensional problem.

6.3.2. Shock-square cylinder interaction. The results for the shock-square cylinder are presented in terms of density contours in Figure 12. Figure 12(a) shows the initial condition in the domain.

DOI: 10.1002/fld

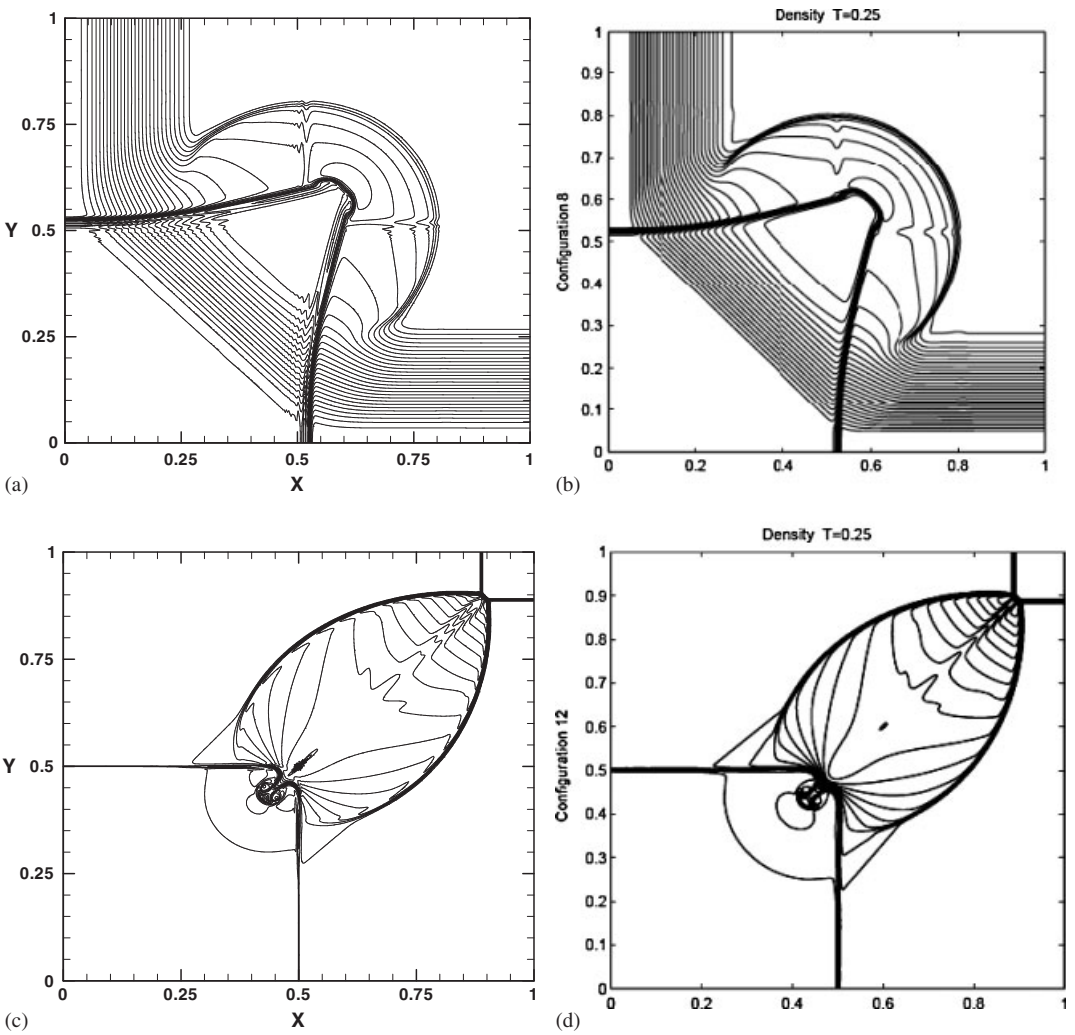

Figure 11. Density contours for two-dimensional Riemann problem after time $t=0.25$ ($\Delta x=0.0025, \Delta y=0.0025$): (a) configuration-8, hybrid method; (b) configuration-8, Lax and Liu [27]; (c) configuration-12, hybrid method; and (d) configuration-12, Lax and Liu [27].

Figure 12(b) gives density variation after time $t=0.1$. At this time, the incident shock is completely reflected from the front face of the cylinder. Figure 12(c) shows density contours at time $t=0.14$, when the reflected shock has moved upstream from the front face of the cylinder and the incident shock has moved to the back face. Figure 12(d) shows the density contours at time $t=0.178$. The incident shock has just started to move over right top and right bottom corner of the cylinder. Figure 12(e) shows the density contour at time $t=0.188$, when the shock has completely passed over the cylinder. Generation of vortices can be seen near the right top and right bottom corners of the cylinder. A comparison with the results obtained for a similar shock diffraction problem by Hillier [28] shows that the hybrid scheme has captured the essential flow features in this interaction.

DOI: 10.1002/fld

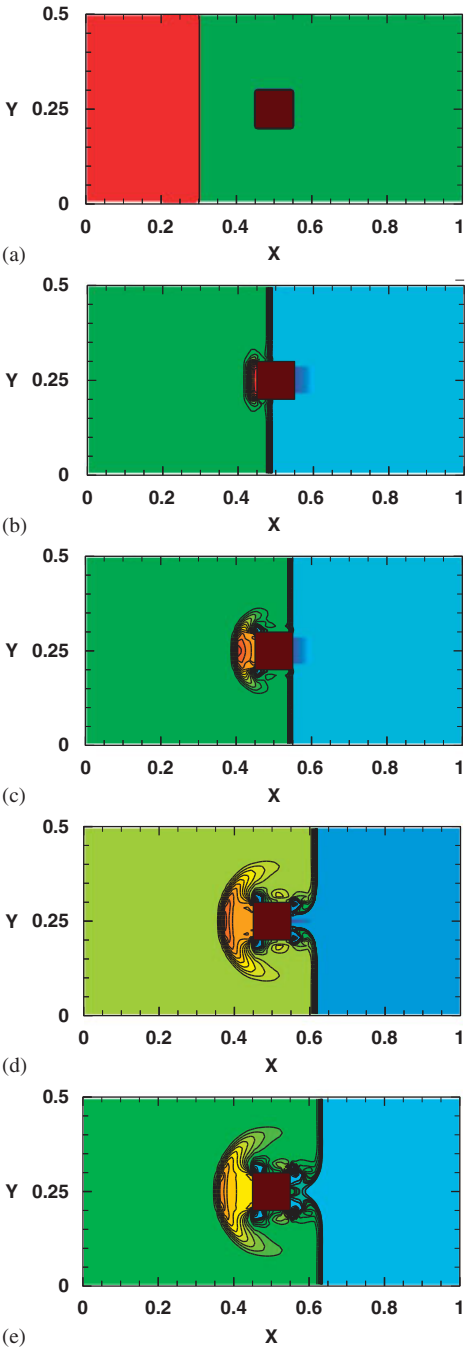

Figure 12. Density contours for shock-square cylinder interaction at times: (a) $t=0$; (b) $t=0.1$; (c) $t=0.14$; (d) $t=0.178$; and (e) $t=0.188$.

DOI: 10.1002/fld

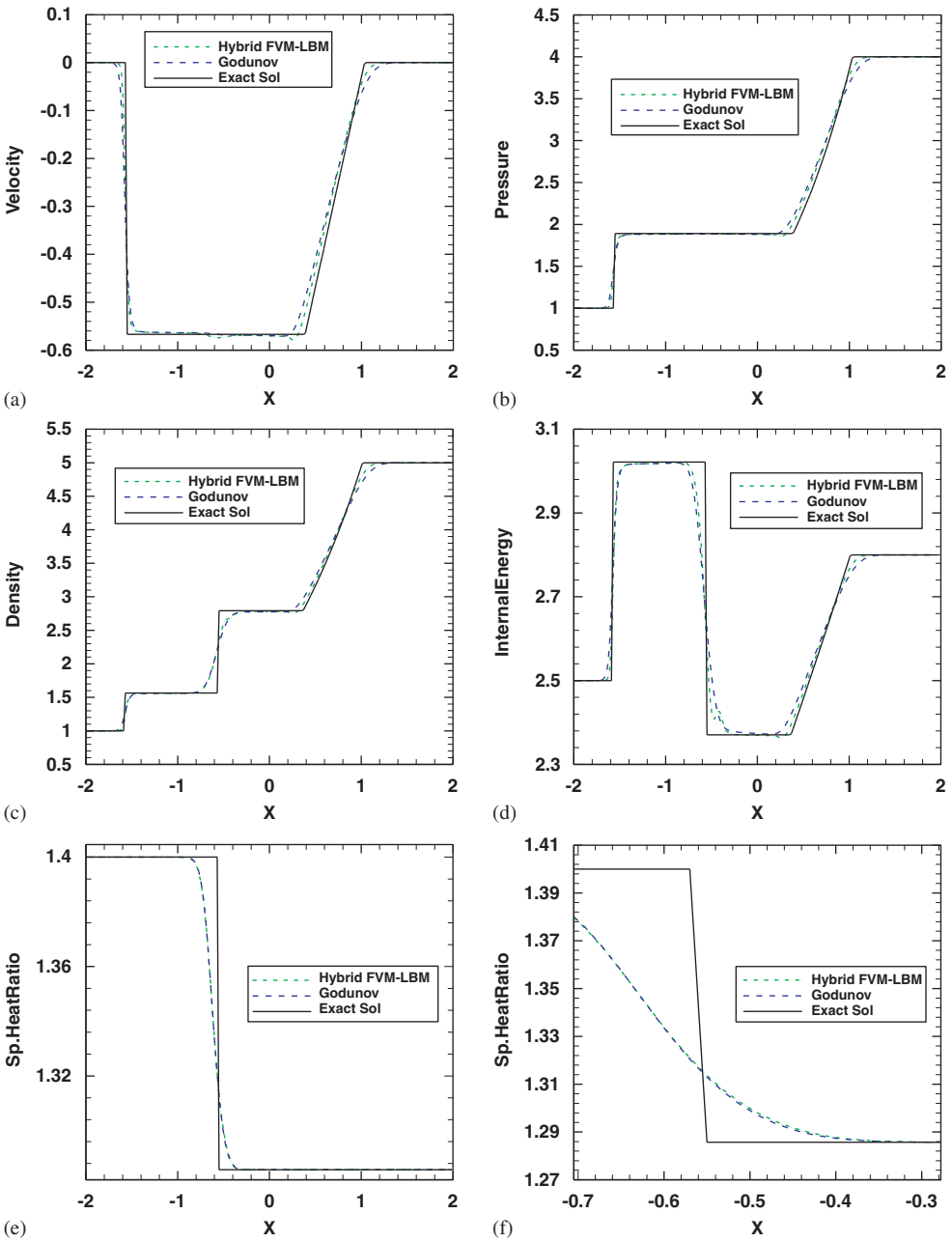

Figure 13. Results for multi-fluid problem after time $t=1$ ($\Delta x=0.02$) for non-dimensional: (a) velocity; (b) pressure; (c) density; (d) internal energy; (e) specific heat ratio 'γ'; and (f) γ (zoomed).

DOI: 10.1002/fld

6.4. Results for multi-fluid compressible flows

The results obtained for a two-gas shock tube are shown in Figure 13. It can be observed that the hybrid method is capable of simulating the shock and contact discontinuity profiles for multi-fluid flows. Furthermore, the hybrid method performs marginally better than the FVM–Godunov method employed for this problem.

7. CONCLUDING REMARKS

A hybrid FVM–LBM method for solving the compressible Euler equations has been proposed in this work. The basic discretization procedure used in this method is the FVM employed on the conservative form of the Euler equations, thus satisfying conservation of mass, momentum and energy. The LBM is used to obtain the inter-cell face fluxes. The hybrid method has been tested on several test cases, both one-dimensional and two-dimensional. The test cases are chosen such that together they have all features of compressible flows: shock, expansion and contact discontinuity. Since satisfactory results have been obtained for all test cases, the proposed hybrid method seems to be sufficiently robust. The hybrid method has been found to typically perform better than the FVM–Godunov scheme and the FVS scheme of Zha and Bilgen. Several important features of the hybrid approach are now outlined. The available LBM models for compressible flows are limited to single fluids. An extension of an earlier LBM model has been proposed and successfully demonstrated on a multi-fluid shock tube problem. The hybrid method has also been applied to non-uniform grids. It is noted that the requirement of a uniform grid is generally cited as an important drawback with LBM. The method has been successfully extended to multi-dimensions. Finally, we propose that using a standard interpolation procedure such as ENO, the variables distribution within a cell can be obtained and the convective derivatives in the particle kinetic equation may be evaluated using a higher-order approximation to ultimately make the scheme higher-order accurate. We note that the current formulation requires that the local Mach number be less than unity—this limitation stems from the use of Kataoka and Tsutahara model. We, however, do not believe that this is a major issue, as the implementation can be improved by choosing a different model. In conclusion, we propose the hybrid scheme as an alternative to the available numerical techniques for simulating a variety of compressible flow problems.

ACKNOWLEDGEMENTS

The second author is grateful to NUS faculty of Engineering for providing travel fund and stay at NUS, Singapore. This work would not have been possible without this visit.

REFERENCES

1. Date AW. *Introduction to Computational Fluid Dynamics* (1st edn). Cambridge University Press: Cambridge, 2005.
2. Toro EF. *Riemann Solvers and Numerical Methods for Fluid Dynamics* (2nd edn). Springer: Berlin, 1999.
3. Godunov SK. A finite difference method for the computation of discontinuous solutions of the equations of fluid dynamics. *Matematicheskii Sbornik* 1959; **47**:357–393.
4. Roe P. Approximate Riemann solvers, parameter vectors and difference schemes. *Journal of Computational Physics* 1981; **43**:357–372.

DOI: 10.1002/fld

5. Roe P, Pike J. Efficient construction and utilization of approximate Riemann solutions. In *Computing Methods in Applied Science and Engineering*, Glowinski R, Lions JL (eds). North-Holland: Amsterdam, 1984.
6. Harten A, Lax P, van Leer B. On upstream differencing and Godunov-type schemes for hyperbolic conservation laws. *Journal of Computational Physics* 1983; **50**:235–269.
7. Toro EF, Spruce M, Spears W. Restoration of the contact surface in the HLL–Riemann solver. *Shock Waves* 1994; **4**:25–34.
8. Steger JL, Warming RF. Flux vector splitting of the inviscid gasdynamic equations with application to finite difference methods. *Journal of Computational Physics* 1981; **40**:263–293.
9. van Leer B. Flux vector splitting for the Euler equations, In *Proceedings of the 8th International Conference on Numerical Methods in Fluid Dynamics*, Krause E (ed.). Springer: Berlin, 1982; 507–512.
10. Liou MS, Steffen CJ. A new flux vector splitting scheme. *Journal of Computational Physics* 1993; **107**:23–39.
11. Liou MS. A sequel to AUSM: AUSM$^+$. *Journal of Computational Physics* 1996; **129**:364–382.
12. Liou MS. A sequel to AUSM, Part II: AUSM$^+$-up for all speeds. *Journal of Computational Physics* 2006; **214**:137–170.
13. Zha GC, Bilgen E. Numerical solutions of Euler equations by using a new flux vector splitting scheme. *International Journal for Numerical Methods in Fluids* 1993; **17**:115–144.
14. Succi S. *The Lattice Boltzmann Equation for Fluid Dynamics and Beyond* (1st edn). Oxford Science Publication: Oxford, 2001.
15. Alexander F, Chen S, Sterling J. Lattice Boltzmann thermohydrodynamics. *Physical Review E* 1993; **47**(4):R2249–R2252.
16. Agarwal A. Novel FVM–LBM for compressible Euler equations. *M. Tech. Thesis*, Department of Mechanical Engineering, Indian Institute of Technology, Bombay, 2007.
17. Alexander FJ, Chen H, Chen S, Doolen GD. Lattice Boltzmann method for compressible fluids. *Physical Review A* 1992; **46**(4):1967–1970.
18. Yu H, Zhao K. Lattice Boltzmann method for compressible flows with high Mach number. *Physical Review E* 2000; **61**(4):3867–3870.
19. Guangwu Y, Yaosong C, Shouxin H. Simple lattice Boltzmann model for simulating flows with shock wave. *Physical Review E* 1999; **59**(1):454–459.
20. Kataoka T, Tsutahara M. Lattice Boltzmann method for compressible Euler equations. *Physical Review E* 2004; **69**:056702.
21. Sun C. Simulations of compressible flows with strong shocks by an adaptive lattice Boltzmann model. *Journal of Computational Physics* 2000; **161**:70–84.
22. Hinton FL, Rosenbluth MN, Wong SK, Lin-Liu YR, Miller RL. Modified lattice Boltzmann method for compressible fluid simulations. *Physical Review E* 2001; **63**:061212.
23. Qu K, Shu C, Chew YT. Alternative method to construct equilibrium distribution functions in lattice-Boltzmann method simulation of inviscid compressible flows at high Mach number. *Physical Review E* 2007; **75**:036706.
24. Clark JF, Karni S, Quirk JJ, Roe PL, Simmonds LG. Numerical computation of two-dimensional unsteady detonation waves in high-energy solids. *Journal of Computational Physics* 1993; **106**:215–233.
25. Jenny P, Mueller B, Thomann H. Correction of conservative Euler solvers for gas mixtures. *Journal of Computational Physics* 1997; **132**:91–107.
26. Wang SP, Anderson MH, Oakley JG, Corradini ML, Bonazza R. A thermodynamically consistent and fully conservative treatment of contact discontinuities for compressible multicomponent flows. *Journal of Computational Physics* 2004; **195**:528–559.
27. Lax PD, Liu XD. Solution of two-dimensional Riemann problems of gas dynamics by positive schemes. *SIAM Journal on Scientific Computing* 1998; **19**(2):319–340.
28. Hillier R. Computation of shock wave diffraction at a ninety degrees convex edge. *Shock Waves* 1991; **1**:89–98.

DOI: 10.1002/fld